Electronic Supplementary Material (ESI) for New Journal of Chemistry.

An Effective Strategy to Construct α-MoO_3//PPy toward High-Energy-Density Asymmetric Supercapacitors

Min Sun [a], Yu Zhang [b], Zhijun Liang [a], Rui Zhang [a], Kai Zhang [a], YanKong Lin [a], Dejun Wang [a] and TengFeng Xie [a], *

[a] College of Chemistry, Jilin University, Changchun 130012, People's Republic of China

[b] Hangzhou Xigu Technology Co., Ltd, Hangzhou 310000.

*Corresponding Author: Tengfeng XIE, Tel: 0431-85168093, E-mail: xietf@jlu.edu.cn

Element	Mo	O
Atom ratio (%)	24.26	75.74

Fig. S1. Mapping images and the corresponding component analysis of the α-MoO_3 powder.

From the data provided by the mapping images, it is clear that the atomic ratio of the elements Mo and O is close to three which is the stoichiometric ratio of MoO_3[1]. This is consistent with our conclusion that only Mo^{6+} appears in the XPS energy spectrum of the Mo 3d orbital.

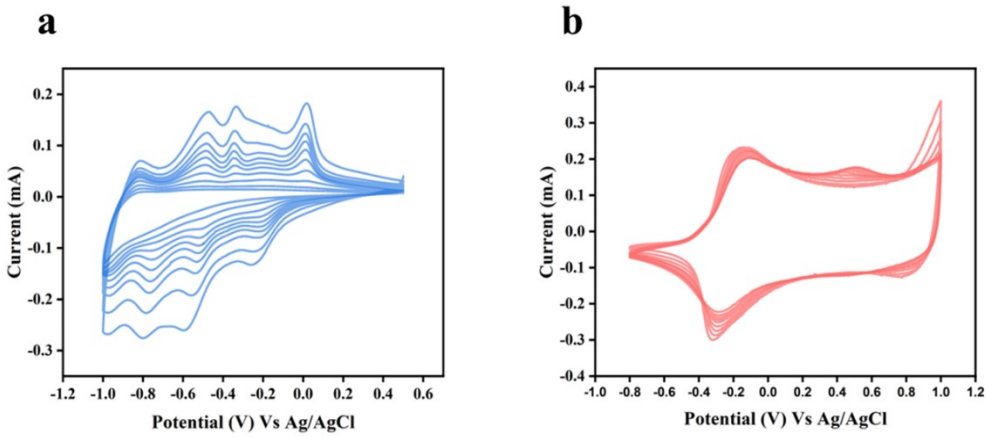

Fig. S2. (a) Multiple cycling of α-MoO_3 at 5 mV/s sweep rate. (b) Multiple cycling of PPy at 5 mV/s scan rate.

With the increase in the number of cycles, the oxidation and reduction peaks of CV curves in the α-MoO_3 were gradually weakened until they disappeared at the 10th cycle, compared to the multi-lap CV cycle of PPy, which always maintained the same shape and almost similar peak areas, which more intuitively indicates that PPy has better stability compared to α-MoO_3, which is conducive to improving the stability of the whole device.

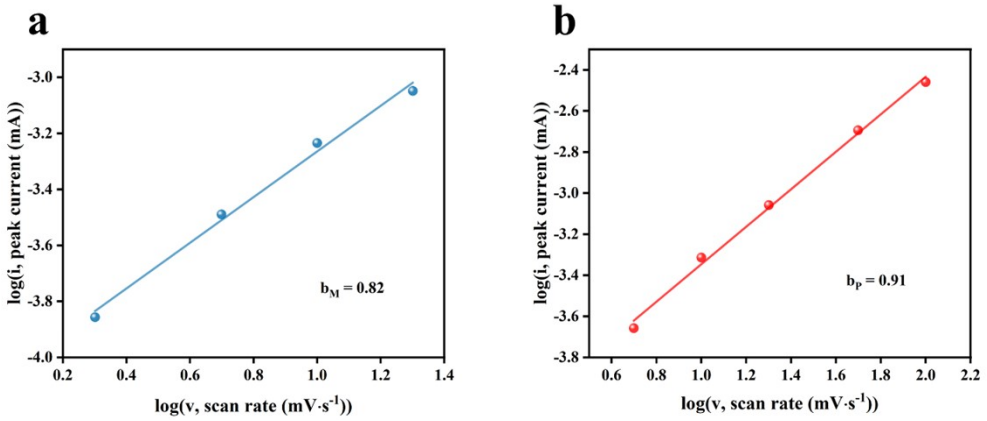

Fig. S3. (a) The log (*i*) *vs.* log (*v*) plots of the anode peak for α-MoO_3 in Fig. 3(a). (b) The log (*i*) *vs.* log (*v*) plots of the cathode peak for PPy in Fig.3(d).

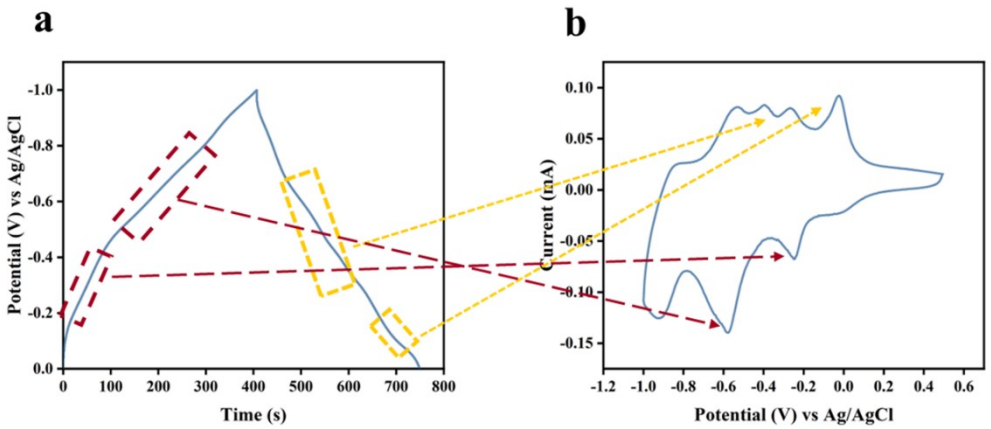

Fig. S4. (a) Charge-discharge curves of α-MoO_3 at a current density of 0.2 mA cm^{-2} under three-electrode conditions. (b) Cyclic voltammetry curves of α-MoO_3 at 2 mV s^{-1} under three-electrode conditions.

Conventional double-layer capacitors exhibit ideal isosceles triangular charge-discharge curves, indicating that capacitance is primarily controlled by the surface. However, MoO_3, as a pseudocapacitive material, displays diffusion-controlled capacitance due to significant oxidation-reduction reactions. According to Gibbs' phase rule, the insertion and extraction of Li^+ ions result in the formation of a homogeneous solid solution, limiting the system's degrees of freedom to 1[2]. Consequently, the galvanostatic charge-discharge (GCD) curve shows a change in chemical potential rather than distinct potential plateaus, reflecting a potential range corresponding to the oxidation-reduction peaks observed in the cyclic voltammetry (CV) curve.

Table S1. Data were obtained based on GCD plots in a three-electrode system, where the area of the electrode material in contact with the electrolyte was 1 cm^2.

Electrode	Mass specific capacitance (F g^{-1})	Potential window (V)	Mass per unit of area (g cm^{-2})
α-MoO_3	623.64	1.0	5.5 × 10-5
PPy	355.56	1.5	7.5 × 10-5

Equations for calculating capacitance based on capacitors:

$$\frac{1}{C_{cell}} = \frac{1}{C_+} + \frac{1}{C_-}$$

Where C_{cell} stands for the capacitance value of the whole system; C_+ and C_- stand for the capacitance values of the anode and cathode materials respectively. As we know, C_{cell} has a maximum value when C_+ equals C_-. Subsequent corrections using the mass of the active material and the applied potential range yielded more accurate equations regarding charge balance:

$$\frac{m_+}{m_-} = \frac{C_- \Delta V_-}{C_+ \Delta V_+}$$

Where m_+ and m_- are the masses of anode and cathode active materials (g), respectively; ΔV_+ and ΔV_- are the applied potential ranges of anode and cathode materials (V), for charging and discharging in the three-electrode system, separately. The data obtained in the above table was brought into the equation of the modified charge balance and it was found that the anode and cathode charge storage capacities were almost the same to get the best quality of the device.

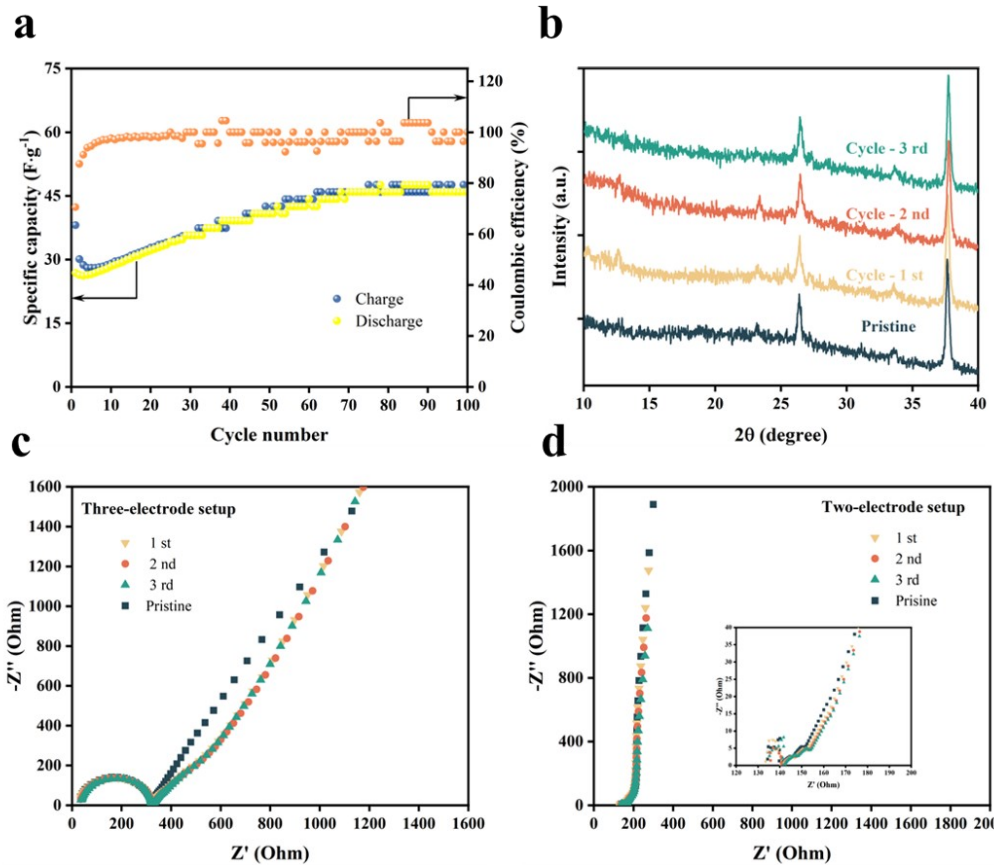

Fig. S5. (a) Cycle stability and Coulombic efficiency (C) of the MoO_3 //PPy system recorded at a current density of 0.5 mA❿cm^{-2}. (b) XRD patterns of both the pristine and cycled MoO_3 samples at various cycling stages. EIS spectrum of (c) MoO_3 in a three-electrode setup and (d) MoO_3//PPy in a two-electrode system measured at Voc after resting for 30min following each complete charge-discharge cycle.

Cyclic stability testing was performed in Fig. S5a at a current density of 0.5 mA❿cm^{-2} in a two-electrode system. It can be observed from the graph that the specific capacitance gradually increases during cycling and eventually reaches a stable value of 46 F❿g^{-1}. This behavior can be attributed to the incomplete activation of the electrode material under high current densities. Go to a further, by analyzing the charging and discharging times for each cycle, the variation in Coulombic efficiency (C) was determined. The initial C in the first cycle was relatively low, around 70.54%, due to incomplete Li^+ insertion and extraction. After 100 cycles, C stabilized at

approximately 100%. The excellent cycle stability can be attributed to two factors: the well-defined and robust nanostructures of both electrodes and the highly reversible Li^+ insertion/extraction process. This conclusion is supported by the analysis of XRD data (Fig. S5b) and EIS data (Fig. S5c & d).

Fig. S5b presents the XRD spectra of MoO_3 following each complete charge-discharge cycle, compared to the pristine state. The spectra exhibit a remarkable similarity, suggesting that the material's crystalline structure remains largely unaltered even after multiple cycles. Specifically, there is no significant change in the inherent structure of the material, and no new peaks associated with Li^+ intercalation are observed[3]. This observation underscores the robustness of the material and its capability for undergoing highly reversible Li^+ insertion and extraction processes during cycling. And we tested the EIS diagram of the MoO_3 material in the different system to reveal the charge and ion transfer properties of electrode materials. Fig. S5c & d show the impedance spectra of the MoO_3 material measured at Voc in three/two-electrode setup after resting for 30min following each complete charge-discharge cycle. The existence of semicircle at a particular angle indicating the charge transfer resistance (Rct) and the steeper slope at low frequency region indicates the capacitive behavior[4]. In Fig. S5c, the nearly constant Rct and the consistent slope in the low-frequency region throughout the cycling process reflect the excellent structural stability of the material and the high reversibility of the Faradaic reactions occurring. Additionally, it is noteworthy that compared to the impedance spectrum of pristine MoO_3, the slope of the curve in the low-frequency region becomes less steep after cycling, which can be attributed to the initially lower Coulombic efficiency, leading to partial Li^+ retention and subsequently reducing the Li^+ diffusion kinetics. Similarly, the impedance data obtained in the two-electrode system reflect the same findings. However, the absence of a distinct semicircle in

the high-frequency region in Fig. S5d indicates a minimal Rct[5]. This can be attributed to the utilization of a PPy electrode, which is a material known for its ability to facilitate rapid charging and discharging processes, thereby enhancing the rate of Faradaic reactions[6].

1. S. N. Lou, N. Sharma, D. Goonetilleke, W. H. Saputera, T. M. Leoni, P. Brockbank, S. Lim, D. W. Wang, J. Scott, R. Amal and Y. H. Ng, *Advanced Energy Materials*, 2017, **7**.
2. B. D. Boruah, B. Wen and M. De Volder, *Nano Letters*, 2021, **21**, 3527-3532.
3. D. Di Yao, M. R. Field, A. P. O'Mullane, K. Kalantar-zadeh and J. Z. Ou, *Nanoscale*, 2013, **5**.
4. T. H. Lee, D. T. Pham, R. Sahoo, J. Seok, T. H. T. Luu and Y. H. Lee, *Energy Storage Materials*, 2018, **12**, 223-231.
5. S. S. Pradeepa, K. Sutharthani, R. Suba Devi, W.-R. Liu and M. Sivakumar, *Journal of the Taiwan Institute of Chemical Engineers*, 2024, **154**.
6. J. Liu, Z. Wang, Q. liu, S. Li, D. Wang and Z. Zheng, *Chemical Engineering Journal*, 2022, **447**.